Research Article

Mehmet Yaşar*, Kadri Kurt, and Ali Yeşil

An innovative approximation concerning the diffusion and electrical conductivity tensor at critical altitudes within the F-region of ionospheric plasma at low latitudes

https://doi.org/10.1515/phys-2025-0227 received January 18, 2025; accepted October 01, 2025

Abstract: This study examines a new method for comprehending diffusion and electrical conductivity tensors in the F-region of ionospheric plasma at low latitudes. The research formulates equations for the real diffusion coefficients by combining electrical conductivity and diffusion processes into a single analytical equation. The coefficients of diffusion and electrical conductivity possess both real and imaginary components as a result of the Earth's real magnetic field configuration. At low latitudes, the constituents of the diffusion tensor display elevated values at night compared to those during the daytime. It has been observed that magnetic diffusion coefficient ratios are minimum in conditions such as equinox days and periods of increased solar activity. This illustrates the impact of solar activity on fluctuations in electron density and ionospheric conductivity. This research examines the equator and demonstrates variability with respect to latitude and temporal factors. The results highlight the influence of the equatorial anomaly on ionospheric diffusion, specifically on the transport of ionized particles caused by the E × B drift, which results in areas of fluctuating electron density. The ultimate goal of this work is to provide numerical evaluations that address a gap in ionospheric transport processes research by integrating diffusion and conductivity into a functional correlation, thus establishing a foundation for future studies.

Keywords: ionosphere, complex diffusion coefficients, electrical conductivity

e-mail: mehmetyasar@firat.edu.tr

Kadri Kurt: Department of Electrical and Energy, Besiri OSB Vocational School, Batman University, Batman, 72000, Turkey

Ali Yeşil: Department of Physics, Science Faculty, Firat University, Elazig, 23270, Turkey

1 Introduction

The ionosphere, the Earth's upper atmosphere, extends from 50 to 1,000 km in altitude. Radio wave propagation is affected by fluctuations in the ionosphere, which is important in radio communications and physics. The most critical parameter of the ionosphere is electron density, which depends on various factors in the ionosphere [1–6]. Geographic, temporal, geomagnetic, and solar factors affect the ionosphere's electron density distribution [7]. Electrons are lighter than ions but have higher average velocities at constant temperatures and are more easily accelerated, making them more mobile [8]. Thus, plasma transfers heat and electric charge primarily through electrons rather than ions. The conductivity and diffusion of a plasma medium are crucial when heat and electrical charge are transferred from one location to another. The ionization levels and solar activity influence the ionosphere's electrical conductivity and diffusion, which are essential. Variations in solar activity are a crucial factor that directly influences ionospheric electron density. The fountain effect escalates dramatically with the increase in solar activity over the years, transporting plasma to altitudes of 1,000 km and enabling diffusion up to approximately 300 km within ±30° geomagnetic latitude [9].

The displacement of charged particles across sites by force or gradient divides the ionosphere into distinct zones [10]. Recent investigations have led to the conclusion that D, the diffusion coefficient, describes how particles or molecules move in a medium over time. A complex diffusion coefficient with real and imaginary components is unstable. Due to the actual diffusion coefficient (Re[D]), thermal motion causes random particle movement. Over time, particles are distributed in space. Increased values of the actual diffusion coefficient indicate a higher concentration of particles in the medium. "Abnormal diffusion" or "bottom diffusion" refers to the imaginary diffusion

^{*} Corresponding author: Mehmet Yaşar, Department of Physics, Science Faculty, Firat University, Elazig, 23270, Turkey,

2 — Mehmet Yaşar *et al.* DE GRUYTER

coefficient. Different diffusion behaviors occur when particles are poorly dispersed and have limited mobility or confinement. A theoretical element in the diffusion coefficient suggests complex interactions or barriers that affect particle mobility during diffusion. The magnitude and measurements of the imaginary component reveal interactions or restrictions. The imaginary component in the diffusion coefficient indicates deviations from standard diffusion patterns, indicating the complexity of a system's diffusion process. Spatial heterogeneity and environmental anomalies can cause particle-media interactions. The diffusion coefficient for ionospheric plasma can be separated into its real and imaginary components. Due to the anisotropy of ionic plasma, diffusion coefficients are tensorial and unique in each direction. Electrical conductivity is crucial to communication and atmospheric sciences. The ionosphere's electrical conductivity relies on numerous variables. Conductivity is both real and imaginary when the motion equation for the ionosphere is solved with respect to the real geomagnetic field geometry in the northern hemisphere of the Earth under the circumstances stated below. The real part of conductivity inverses resistance, while the imaginary part inverses reactance [3,8,11-18].

In this regard, significant and scientifically pioneering studies have been carried out on the conductivity and diffusion of the ionosphere. However, studies on conductivity and diffusion are limited in the context of ionospheric research. Specifically, anisotropic ionosphere plasma, which is both conductive and fluid, validates the equations used for fluid dynamics and electrical conductivity. In this case, the conductivity and diffusion coefficients in the ionosphere plasma have a complex and tensorial structure. None of the previous studies have accounted for the above-mentioned situation, nor have they established a functional relationship between conductivity and diffusion. Some of the studies conducted on this subject in recent years are as follows. Various statistical studies have been conducted on the equatorial ionosphere effects in the past. Aggarwal et al. [19], Mo and Zhang [20], Oluwadare et al. [21], and Mridula et al. [22] conducted studies on the equatorial ionosphere anomaly in different time periods and different regions using total electron content data observed at the Global Positioning System (GPS) station. Apart from these, there are also studies on a global scale. Li et al. used the FORMOSAT-3/COSMIC satellite constellation in three-dimensional modeling of the low latitude ionosphere and detected rich structural changes in the equatorial anomaly [23]. Li et al. used the DMSP satellite in a study on the formation rates of the equatorial anomaly at night-time from 2000 to 2002 [24]. Nigussie et al. conducted a study to model the equatorial anomaly during daytime from 2014 to 2018 using global in-situ ion density data from Swarm A and NmF2 data from COSMIC-1 [25].

First, the study of the low-latitude ionosphere using certain satellite constellations is limited by their own constraints. While satellites provide high spatial and temporal resolution when passing over the equator, data collection becomes limited when they move away from the equator. This causes gaps in observations at certain times, preventing full observation of low-latitude regions and the equator at all times. On the other hand, in comprehensive studies on the low-latitude ionosphere, periods of high solar activity should be selected.

This study aims to build on previous research efforts. One of its main objectives is to establish a functional relationship between the electrical conductivity and diffusion coefficient of both transport processes, as well as to emphasize that both have a complex structure when real conditions are considered. In this study, electrical conductivity and diffusion are combined into a single mathematical equation (Eq. (14)) derived without any approximation, forming a basis for future studies. An analytical model that can be used in ionosphere and near-earth space studies has been developed, and the main objective of the study has been achieved.

2 Electron diffusion equations for ionospheric plasma under unstable conditions

Considering the ionospheric plasma as a collection of particles consisting of neutrals, electrons, and ions and adopting the approach that the sizes of plasma irregularities are smaller than all the characteristic scale sizes of the plasma, we can use the magnetohydrodynamic approach for all components of the ionospheric plasma. This condition can be described by the continuity and motion equations of charged particles. For heights above region E, as in fluid mechanics, these equations can be written as follows [1,4,10]:

$$\frac{\partial N_a}{\partial t} + \nabla \cdot \mathbf{j}_a = 0, \tag{1}$$

$$\frac{\partial N_{\rm m}}{\partial t} + \nabla \cdot (U_{\rm m} N_{\rm m}) = 0, \qquad (2)$$

where $\alpha = e, i$, and m represent electrons, ions, and neutral particles, respectively; N represents the concentration of particles; J represents the electrical conductivity; U represents the average particle velocity. Based on these, the electron and ion current densities are as follows [1,15]:

$$\mathbf{j}_{e} = -\frac{\widehat{\sigma}_{e}}{e} \left\{ \mathbf{E} + \left[\mathbf{U}_{m} \, \mathbf{B}_{0} \right] \right\} - \widehat{D}_{ee} \nabla N_{e} - \widehat{D}_{Te} \frac{N_{e}}{T_{e}} \nabla T_{e} + N_{e} \mathbf{U}_{m}, \quad (3)$$

$$\mathbf{j}_{\mathbf{i}} = \frac{\widehat{\sigma}_{\mathbf{i}}}{e} \{ \mathbf{E} + [\mathbf{U}_{\mathbf{m}} \mathbf{B}_{\mathbf{0}}] \} - \widehat{D}_{\mathbf{i}\mathbf{i}} \nabla N_{\mathbf{i}} - \widehat{D}_{T\mathbf{i}} \frac{N_{\mathbf{i}}}{T_{\mathbf{i}}} \nabla T_{\mathbf{i}} + N_{\mathbf{i}} \mathbf{U}_{\mathbf{m}}, \quad (4)$$

where $\sigma_{\rm e}$ and $\sigma_{\rm i}$ are the conductivity tensor for electron and ion, D_e and D_i are the diffusion tensor for electron and ion, N_e and N_i are the particle density for electron and ion, $T_{\rm e}$ and $T_{\rm i}$ are the particle temperature for electron and ion, E is the electric field, B_0 is the magnetic field, and $U_{\rm m}$ is the neutral particle velocity.

$$M_{\rm m}N_{\rm m} \left[\frac{\partial \mathbf{U}_{\rm m}}{\partial \mathbf{t}} + (\mathbf{U}_{\rm m}\nabla) \mathbf{U}_{\rm m} \right]$$

$$= -\nabla (N_{\rm m}T_{\rm m}) \frac{\widehat{\sigma}_{\rm e}}{e} - \eta U_{\rm m} - \frac{1}{3}\eta (\mathbf{U}_{\rm m})$$

$$- m\widehat{v}_{\rm em}(N_{\rm e}\mathbf{U}_{\rm m} - \mathbf{j}_{\rm e}) - M_{\rm i}\widehat{v}_{\rm im}(N_{\rm i}\mathbf{U}_{\rm m} - \mathbf{j}_{\rm i}),$$
(5)

where $M_{\rm m}$ is the total mass for neutral particles and η is the viscosity coefficient for any particle.

When any irregularity occurs in the ionospheric plasma, an electric field is generated due to charge separation, and a magnetic field associated with this electric field is formed. These are described by Maxwell's equations as follows:

$$\nabla \cdot \mathbf{E} = e(N_{\rm i} - N_{\rm e}),\tag{6}$$

$$\nabla \times \mathbf{E} = -\frac{\partial \mathbf{B}}{\partial \mathbf{t}},\tag{7}$$

$$\nabla \cdot \mathbf{B} = 0, \tag{8}$$

$$\nabla \times B = e(\mathbf{j}_i - \mathbf{j}_a). \tag{9}$$

When the above equations are used together, the diffusion tensor based on conductivity is as follows [1]:

$$\widehat{D}_{ee} = \widehat{D}_{e} \left[1 + \frac{T_{i}}{T_{e}} \right] - \frac{T_{e}}{e^{2} N_{e}} \widehat{\sigma}_{e}, \tag{10}$$

where D_{ee} is the diffusion tensor related to conductivity for electrons, D_e is the diffusion tensor for electron, and e is the electron charge.

When the Earth's actual magnetic field geometry is used for the Northern Hemisphere, the magnetic field components are

$$\mathbf{B} = B_{\mathbf{v}}\mathbf{i} + B_{\mathbf{v}}\mathbf{i} + B_{\mathbf{z}}\mathbf{k},\tag{11}$$

where $B_x = B \cos I \sin d$, $B_y = B \cos I \cos d$, $B_z = -B \sin I$, *I* is the magnetic dip, and *d* is the angle of magnetic declination. The other rotations to be used in this study are as follows: ω_c is the cyclotron frequency. The frequencies that depend on the plasma parameters are given as follows [10]:

$$\omega_{cx} = \frac{eB_{x}}{m}, \ \omega_{cy} = \frac{eB_{y}}{m} \text{ and } \omega_{cz} = \frac{eB_{z}}{m},$$

$$D_{e} = \begin{bmatrix} D_{xxR} & D_{xyR} & D_{xzR} \\ D_{yxR} & D_{yyR} & D_{yzR} \\ D_{zxR} & D_{zyR} & D_{zzR} \end{bmatrix} + i \begin{bmatrix} D_{xxI} & D_{xyI} & D_{xzI} \\ D_{yxI} & D_{yyI} & D_{yzI} \\ D_{zxI} & D_{zyI} & D_{zzI} \end{bmatrix}.$$
(12)

For the same geometry, the conductivity tensor is also complex [7,10,15,26,27]:

$$\sigma_{e} = \begin{bmatrix} \sigma_{xxR} & \sigma_{xyR} & \sigma_{xzR} \\ \sigma_{yxR} & \sigma_{yyR} & \sigma_{yzR} \\ \sigma_{zxR} & \sigma_{zyR} & \sigma_{zzR} \end{bmatrix} + i \begin{bmatrix} \sigma_{xxI} & \sigma_{xyI} & \sigma_{xzI} \\ \sigma_{yxI} & \sigma_{yyI} & \sigma_{yzI} \\ \sigma_{zxI} & \sigma_{zyI} & \sigma_{zzI} \end{bmatrix}.$$
(13)

When Eqs. (13) and (12) are substituted into Eq. (10), neglecting the displacement current, the complex electron diffusion coefficient for the quasi-steady state is

$$\widehat{D}_{ee} = \begin{bmatrix} D_{exxR} & D_{exyR} & D_{ezzR} \\ D_{eyxR} & D_{eyyR} & D_{eyzR} \\ D_{ezxR} & D_{ezyR} & D_{ezzR} \end{bmatrix} + i \begin{bmatrix} D_{exxI} & D_{exyI} & D_{exzI} \\ D_{eyxI} & D_{eyyI} & D_{eyzI} \\ D_{ezxI} & D_{ezyI} & D_{ezzI} \end{bmatrix}. (14)$$

3 Numerical analysis and results

This study examines the diffusion tensor of electrons at low amplitudes inside the F-region altitudes of the ionosphere (390, 410, and 450 km) at 12:00 LT and 24:00 LT under unstable conditions. It primarily focuses on the scenario outlined in Eq. (10), where the displacement current is neglected and quasi-stationary methods are used for density and temperature. Taking these techniques into account, the diffusion equation is formulated based on electrical conductivity. It should be noted that the diffusion coefficient is not singular; it comprises both real and imaginary components. This is predicated on the assumption that the dynamics and distribution of ions and free electrons are essential for understanding the highest layer of the Earth's atmosphere - ionosphere.

Many events affect electron density both inside and outside the ionosphere. Electron density varies hourly, daily, monthly, and yearly. If a scientific study related to the ionosphere is to be conducted, many variables must be considered together. Therefore, especially in theoretical studies, the necessity to impose certain restrictions arises. The conditions considered in this article are as follows:

1) Sunspot numbers provide key insights into the Sun's 11year activity cycle, influencing solar radiation, space weather, and potentially even terrestrial climate. These numbers help scientists predict solar events like solar flares and geomagnetic storms, which can impact satellite systems, communications, and power infrastructure on Earth. Monitoring the sunspot numbers and understanding the solar cycle are crucial for preparing for space weather and understanding the Sun's broader influence on the solar system. This study focuses on the year 1990, when the sunspot activity was at its maximum.

- 2) The behavior of the F-region differs at low latitudes. For example, the electron density at midnight is greater than that in the afternoon hours. This is contrary to what is expected and is known as the equatorial anomaly in the ionosphere. The equatorial ionization anomaly is primarily driven by the equatorial plasma fountain effect, where ionized particles are lifted to higher altitudes by electric fields (E × B drift) and then diffuse along magnetic field lines to lower latitudes. This creates two crests of high electron density around ±15° magnetic latitude and a trough at the magnetic equator. The irregular distribution of ionization density affects radio wave propagation and global navigation satellite systems signals, causing challenges for both space- and ground-based communication systems.
- 3) Equinox days are the days when the Earth's axis is tilted at zero degrees relative to the Sun's rays as it revolves around the Sun, meaning the Sun's rays hit the equator perpendicularly. During these days, the durations of night and day are almost equal. Equinox, by definition, means "equal night." Equinoxes occur twice a year, on March 21 and September 23.
- 4) The electron transport in the ionosphere is related to the movement of electrons, and this movement occurs particularly due to electrical currents and the influence of magnetic fields. Electrons can move freely in this environment, and this movement leads to various physical phenomena. The movement of electrons in the ionosphere varies depending on factors such as solar activity and the magnetic field. The movement of electrons in the ionosphere is a complex process influenced by factors such as solar radiation and the magnetic field. This process leads to the formation of many phenomena such as radio waves, GPS signals, auroras, and space weather. In this study, the ionosphere's conductivity and diffusion equations were combined into a single equation, using the Earth's actual magnetic field geometry in the Northern Hemisphere (Eq. (10)).

Since the ionosphere has an unstable structure, the conductivity and diffusion coefficients have a complex structure. The real part of conductivity is the inverse of resistance, while the imaginary part is the inverse of reactance. It refers to the proper transmission of electric current within the ionosphere. Specifically, it represents the direct conductivity of the ionosphere when an electrical field is applied. The imaginary part, on the other hand, is

related to processes such as energy storage and release (e.g., capacitive losses) and is defined as reactive power. The real diffusion coefficient explains how the density of substances changes over time and the rate of diffusion. The imaginary part of diffusion is related to phase shift and energy storage. This generally refers to wave-like diffusion or delayed diffusion processes.

According to the conditions outlined earlier, the calculations for Eq. (10) were made separately for the real and imaginary parts. The squares of the real and imaginary parts were then taken to obtain the square root. For each height, the average values of the tensor elements calculated at low latitudes were obtained for 12:00 and 24:00 LT, as their values were close to each other. Accordingly, the graph of the average diffusion coefficients at low latitudes is given in Figure 1. According to Eq. (14), the magnitudes of the diagonal elements of the matrix are almost equal to each other. There is a rapid linear decrease from south to north, reaching a minimum of -5°S, followed by an increase up to 5°N, with constant values between 5°N and 10°N. After this latitude, there is another decrease to about 20°N, followed by an increase starting from that point. $D_{yx} = D_{xy}$. The change in these elements is an exponential decrease of 5°N to the north, then an exponential increase after the latitude. However, the behavior of D_{xx} differs. This tensor element decreases up to -5°S, increases between 0° and 10°N, and then its magnitude decreases exponentially after this latitude. $D_{vz} = D_{zv}$, where D_{vz} and D_{zv} are approximately equal in magnitude and exhibit similar behavior with latitude to the diagonal elements of the tensor. As shown in Figure 1, at 24:00 LT, the behavior of each tensor element is generally similar to the other. However, the values of all tensor elements are higher compared to those at 12:00 p.m. LT.

Figure 2 presents the variation of average diffusion coefficients with latitude for September 23. The trend in this figure is very similar to that of Figure 1. That is, there are increases between the same latitudes for both 12:00 LT and 24:00 LT; maxima and minima occur at the same latitudes. Based on the figures and the obtained numerical values, it can be said that on September 23, the numerical values of all tensor elements show a slight increase.

In the study conducted by Pignalberi *et al.*, the effective scale height modeled by means of the Epstein layer is mathematically related to the vertical scale height theoretically derived from the plasma ambipolar diffusion theory. The connections have been previously demonstrated by calculating effective scale height values from the COSMIC/FORMOSAT-3 radio dataset. The relationship between the vertical slope of the topside scale height obtained from the COSMIC/FORMOSAT-3 satellite and the electron temperature obtained from the ESA Swarm B

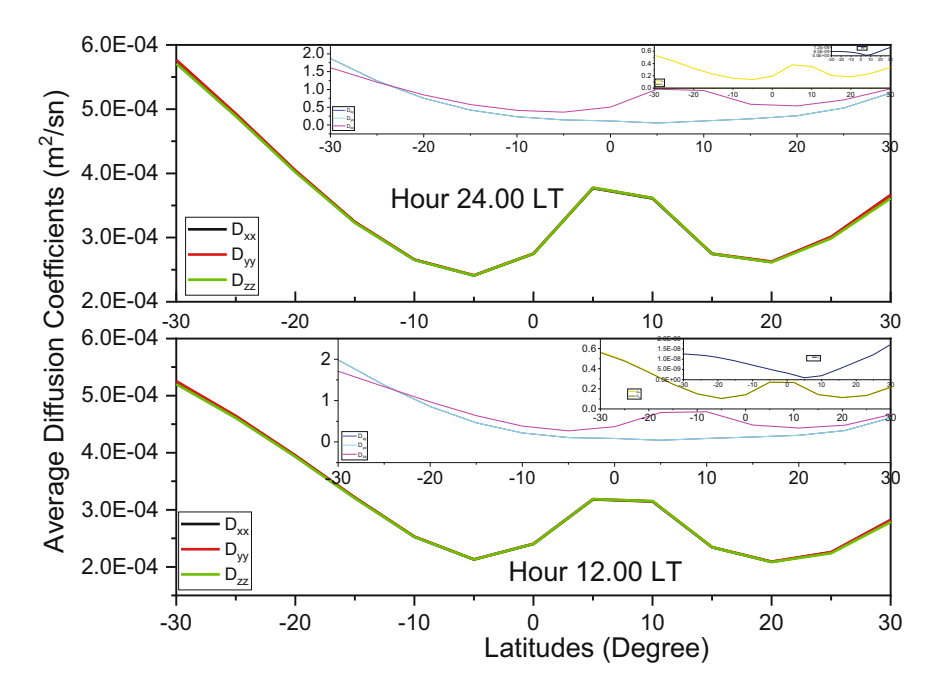


Figure 1: Variation of average diffusion coefficients with latitude (March 21, 12:00 and 24:00 LT).

satellite was investigated with respect to diurnal, seasonal, solar activity, and latitudinal variations. It was found that both satellites show very similar daily, seasonal, and solar activity trends as a function of magnetic latitude on the *y*-axis. It is also suggested that the proposed methodology can help improve the upper surface description provided by ionospheric models, such as NeQuick and IRI [28].

Similar to the study of Pignalberi *et al.* (2020), which focused on variations such as the diurnal, seasonal, solar activity, and latitudinal effects, the results of this study were obtained by selecting the equinox days at low latitudes in 1990, when sunspot activity was at its maximum. In line with the idea that the results from two different satellites can contribute to the studies using ionospheric

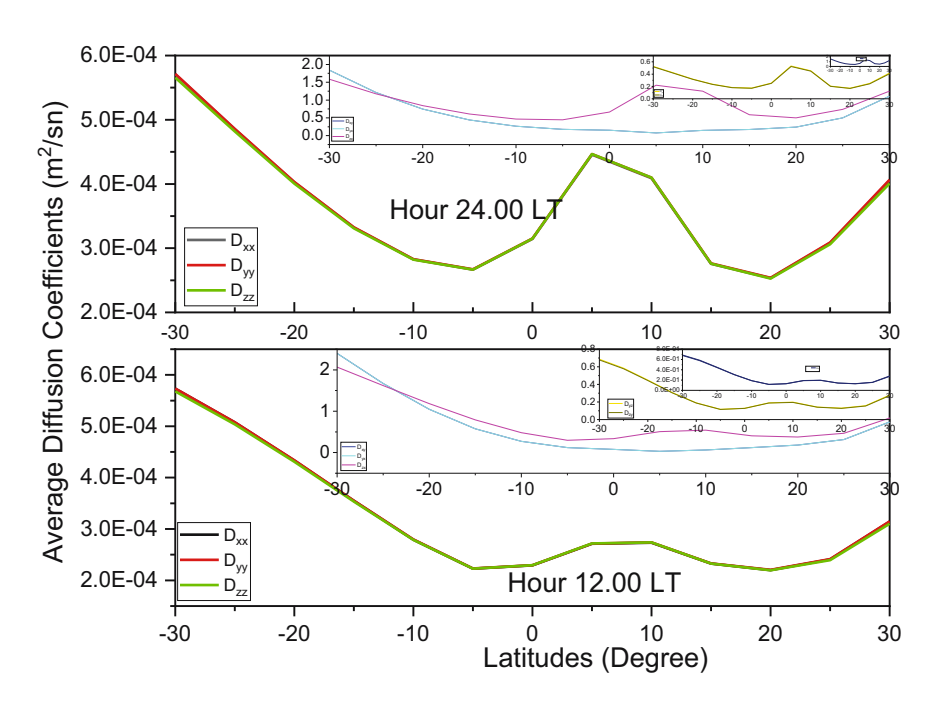


Figure 2: Variation of average diffusion coefficients with latitude (September 23, 12:00 and 24:00 LT).

models such as NeQuick and IRI, this study aims to contribute to the understanding of the physical properties of the upper ionosphere by using the IRI model.

In the study by Vaishnav *et al.*, titled "Role of eddy diffusion in the delayed ionospheric response to solar flux changes," the combined effects of eddy diffusion and solar activity show a greater delay in the low- and mid-latitude regions, suggesting that eddy diffusion plays an important role in ionospheric delay. Therefore, additional numerical modeling and observational results are required to better understand the role of lower atmospheric forcing and thermosphere—ionosphere coupling [29].

In this study, calculations were made by selecting low latitudes and high solar activity, in accordance with the study by Vaishnav *et al.* [29]. While the diffusion rate is expected to be higher during the day than at night, the opposite was observed. These trends can be clearly seen in Figures 1 and 2. The reason for this may be the equatorial anomaly such as fluctuations in the electron density of the ionospheric F region around the equator and the transport of plasma from the equator to the north and south due to the vertical $E \times B$ drift in the equatorial region. As noted by Vaishnav *et al.* [29], in addition to observation and simulation studies, the results based on the numerical calculations conducted in this study will contribute to a better understanding of the role of lower atmospheric forcing and thermosphere-ionosphere coupling.

Balan *et al.* stated in their studies that the equatorial plasma source causes the field-perpendicular $E \times B$ plasma drift and field-aligned plasma diffusion to act together, causing the plasma to flow along the field lines at all heights. The ionization anomaly at the equator occurs due to the $E \times B$ drift, and the plasma at the equator diverges, which creates troughs and peaks. When the peaks are within $\pm 20^\circ$ magnetic latitudes, there is a small plasma accumulation at the peaks, and when they are beyond $\pm 25^\circ$ magnetic latitudes, there is no accumulation [30].

In Figures 1 and 2, troughs and peaks were observed due to latitudinal changes. In our study, pits and hills were observed up to ±20° latitude in Figure 1, which represents March 21, and Figure 2, which represents September 23. These pits and hills are thought to have formed due to reasons originating from the equatorial anomaly, in accordance with the results obtained by Balan *et al.* [30].

4 Conclusions

The numerical analysis indicates that diffusion rates at low latitudes are higher in the southern hemisphere than in the

northern hemisphere, and the magnitudes of the diagonal elements of the tensor are less than those of the off-diagonal elements, with the D_{zx} element exhibiting the smallest value. Diffusion rates are minimal at the equator, remain fairly stable between 5°N and 150°N, and then undergo a sharp decline at 200°N. The results show that diffusion rates at night are higher than those during the day, and the diffusion rates on September 23 exceeded those on March 21. Furthermore, during both seasons, at 12:00 and 24:00 local time, the diagonal components of the tensor exhibit values comparable to the magnitude of the ionosphere's electrical conductivity. The values in the conductivity tensor strongly influence the diffusion rates, considerably reducing their magnitudes. Moreover, this perspective distinguishes itself from earlier research by employing IRI data, a semi-empirical approach for observing the low-latitude ionosphere, and by representing electrical conductivity and diffusion in a single tensor equation.

In this study, a comprehensive analytical equation connecting the diffusion and electrical conductivity tensors in the F region of the ionospheric plasma at low latitudes is effectively formulated by integrating the real geometry of the Earth's magnetic field. Both diffusion and conductivity coefficients were determined to comprise real and imaginary components. The real component signifies standard diffusion and conductivity, but the imaginary component denotes deviations resulting from spatial heterogeneity and environmental anomalies. The diagonal components of the diffusion tensor exhibited values akin to the magnitude of ionospheric conductivity, whereas the other tensor components demonstrated markedly elevated values. The equatorial anomaly was recognized as a contributing factor to these fluctuations. Fluctuations in diffusion coefficients were noted near ±20° latitude, indicating the impact of ionized particle transport resulting from vertical $E \times B$ drift in the equatorial zone. The results for the equinox days (March 21 and September 23) exhibited analogous latitudinal patterns in diffusion behavior.

This innovative methodology that integrates conductivity and diffusion into a unified equation (Eq. (14)) establishes a foundation for subsequent theoretical investigations and practical implementations, including the refinement of ionospheric models and the enhancement of forecasts regarding space weather effects on communication systems. This model will form the basis for future studies, but since there are many variable parameters of the ionosphere, restrictions similar to those used in this model may be necessary. In addition, although numerical calculations are made only for electrons, this approach also allows for the calculation of ions in the ionosphere.

Funding information: The authors state no funding involved.

Author contributions: All authors have accepted responsibility for the entire content of this manuscript and approved its submission.

Conflict of interest: The authors state no conflict of interest.

Data availability statement: All data generated or analyzed during this study are included in this published article.

References

- Ojichukwu EB, Uda CN. The analysis of variation of electromagnetic wave propagation in D- and F-Layers of ionosphere. World Sci News. 2023;186:124-38.
- Yaşar M. The solar eclipse effect on diffusion processes of $O^+ + O_2$ → O₂ + O reaction for the upper ionosphere over Kharkov. Therm Sci. 2021;25(1):S57-63.
- Rishbeth H. A review of ionospheric F region theory. Proc IEEE. 1967;55(1):16.
- [4] Saakian A. Radio wave propagation fundamentals. Second edition. London: Artech House; 2021.
- Niknam K, Simpson JJ. A review of grid-based, time-domain modeling of electromagnetic wave propagation involving the ionosphere. IEEE J-MMCT. 2021;6:214-28.
- Panasenko SV, Aksonova KD, Kotov DV. Characteristics of Traveling Ionospheric Disturbances from Incoherent Scatter Data. Dallas: Primedia eLaunch LLC: 2021.
- Timoçin E, Yeşil A, Ünal İ. The effect of the geomagnetic activity to the hourly variations of ionospheric foF2 values at low latitudes. Arab. J Geosci. 2014;7(10):4437-42.
- Evangelias A. Equilibrium and stability of helically symmetric magnetized plasmas. Ionnina: University of Ionnina; 2020.
- He L, Zhu Q, Wang C. Comprehensive analysis of the equatorial ionization anomaly based on global ionospheric maps with a high spatiotemporal resolution. Adv Space Res. 2024;74(8):3511–26.
- [10] Sağır S, Yeşil A, Sanac G, Ünal İ. The characterization of diffusion tensor for mid-latitude ionospheric plasma. Ann Geophys. 2014;57(2):A0216.
- [11] Pécseli HL. In waves and oscillations in plasmas. 2nd edn. Oxon: CRC Press; 2020. p. 225-38.
- [12] Gómez Míguez MM, Martínez Gómez D, Khomenko E, Vitas N. The influence of thermal pressure gradients and ionization (im)balance on the ambipolar diffusion and charge-neutral drifts. Philos Trans R Soc A. 2024;382(2272):20230228.
- [13] Hysell DL, Fang TW, Fuller-Rowell TJ. Modeling equatorial F-region ionospheric instability using a regional ionospheric irregularity

- model and WAM-IPEJ. Geophys Res Space Phys. 2022;127(9):e2022JA030513.
- [14] Ata-ur-Rahman A, Khalid M, Eldin SM. Oblique propagation of arbitrary amplitude ion acoustic solitary waves in anisotropic electron positron ion plasma. Front Phys. 2023;11:1144175.
- [15] Rishbeth H, Garriott OK. Introduction to ionospheric physics. Amsterdam: Academic Press; 1969.
- [16] Chowdhury S, Kundu S, Basak T, Ghosh S, Hayakawa M, Chakraborty S, et al. Numerical simulation of lower ionospheric reflection parameters by using International Reference Ionosphere (IRI) model and validation with Very Low Frequency (VLF) radio signal characteristics. Adv Space Res. 2021;67(5):1599-2251.
- Yeşil A, Özcan O, Inc M, Sağir S, Kurt K, Tsamalashvili LV, et al. The change of the magnitude of the electric field vector (Ev/E0) in the ionosphere in the magnetic equator through. Türk J Sci Technol. 2021;16(1):31-8.
- [18] Kurt K. The seasonal behavior of the characteristic wave in low latitudes. Int J İnnov Eng Appl. 2021;5(1):36-9.
- [19] Aggarwal M, Joshi HP, Iyer KN, Kwak Y-S, Lee JJ, Chandra H, et al. Day-to-day variability of equatorial anomaly in GPS-TEC during low solar activity period. Adv Space Res. 2012;49:1709-20.
- Mo X, Zhang DA. Comparative study of the northern and southern equatorial ionization anomaly crests in the East-Asian sector during 2006-2015. Adv Space Res. 2021;68:1461-72.
- Oluwadare TS, Nguyen Thai C, Akala AO-O, Heise S, Alizadeh M, Schuh H. Characterization of GPS-TEC over African equatorial ionization anomaly (EIA) region during 2009-2016. Adv Space Res. 2019;63:282-301.
- Mridula N, Pant TK, Manju G. On the variability of the equatorial [22] ionization anomaly trough over Indian region: a novel analysis using Beacon TEC measurements. Adv Space Res. 2020;66:646-54.
- [23] Li G, Ning B, Liu L, Ren Z, Lei J, Su SY. The correlation of longitudinal/seasonal variations of evening equatorial pre-reversal drift and of plasma bubbles. Ann Geophys. 2007;25:2571-8.
- [24] Li J, Chen Y, Liu L, Le H, Zhang R, Huang H, et al. Occurrence of ionospheric equatorial ionization anomaly at 840 km height observed by the DMSP satellites at solar maximum dusk. Space Weather. 2021;19(5):1-13.
- [25] Nigussie M, Jakowski N, Hogue M. Characterization and climatological modeling of equatorial ionization anomaly (EIA) crest position. J Geophys Res Space Phys. 2022;127(12):1-10.
- [26] Timoçin E, Yeşil A, Ünal İ. The responses of ionospheric conductivities on the mid-latitudes to changes in the BZ component of interplanetary magnetic field. Wireless Pers Commun. 2020;114(4):2923-32.
- [27] Yesil A, Kurt K. Calculation of electric field strength in the ionospheric F-region. Therm Sci. 2018;22(1):159-64.
- Pignalberi A, Pezzopane M, Nava B, Coïsson P. On the link between the topside ionospheric effective scale height and the plasma ambipolar diffusion, theory and preliminary results. Sci Rep.
- Vaishnav R, Jacobi C, Berdermann J, Codrescu M, Schmölter E. Role [29] of eddy diffusion in the delayed ionospheric response to solar flux changes. Ann Geophys. 2021;39(4):641-55.
- Balan N, Liu L, Le H. A brief review of equatorial ionization anomaly [30] and ionospheric irregularities. EPP Space Phys. 2018;2(4):257-75.

Appendix

a) Tensor elements of diffusion coefficients

$$\begin{split} D_{XXXR} &= \frac{(u_3^3 u_3^2 + \omega_{Ca}^2 + 2\omega_{Ca}^2 + 2\omega_{Ca}^2) + v_a[(\omega_{Ca}^2 - \omega_a^2) + 4v_a^2\omega^2]}{(\omega^2 + v_a^2)[((\omega_{Ca}^2 + v_a^2 - \omega^2) + 4v_a^2\omega^2]} \\ D_{XXXII} &= \left[\frac{v_2^2 \omega(v_a^2 - \omega_{Ca}^2 + 3\omega_{Caa}^2 + 2\omega^2) + \omega(\omega_{Ca}^2 - \omega^2)(\omega_{Caa}^2 - \omega^2)}{((\omega^2 + v_a^2)((\omega_{Ca}^2 + v_a^2 - \omega^2) + 4v_a^2\omega^2]} \right], \\ D_{XXII} &= \frac{(\omega_{CXX}\omega_{CYX}u_a(\omega_{Ca}^2 + v_a^2 - 3\omega^2) - \omega_{CXI}(v_a^2 + w^2)(\omega_{Ca}^2 + v_a^2 - \omega^2)}{((\omega^2 + v_a^2)[((\omega_{Ca}^2 + v_a^2 - \omega^2) + 4v_a^2\omega^2]]} \\ D_{XXII} &= \frac{(\omega_{CXX}\omega_{CYX}\omega_a(\omega_{Ca}^2 + 3v_a^2 - \omega^2) - \omega_{CXI}(v_a^2 + \omega^2)(\omega_{Ca}^2 + v_a^2 - \omega^2)}{((\omega^2 + v_a^2)[((\omega_{Ca}^2 + v_a^2 - \omega^2) + 4v_a^2\omega^2]]} \\ D_{XXII} &= \frac{-\omega_{CXX}\omega_{CXX}u_a(\omega_{Ca}^2 + v_a^2 - 3\omega^2) - \omega_{CXI}(v_a^2 + \omega^2)(\omega_{Ca}^2 + v_a^2 - \omega^2)}{((\omega^2 + v_a^2)[((\omega_{Ca}^2 + v_a^2 - \omega^2) + 4v_a^2\omega^2]]} \\ D_{XXII} &= \frac{-\omega_{CXX}\omega_{CXX}u_a(\omega_{Ca}^2 + 3v_a^2 - 3\omega^2) - \omega_{CXX}(v_a^2 + \omega^2)(\omega_{Ca}^2 + v_a^2 - \omega^2)}{((\omega^2 + v_a^2)[((\omega_{Ca}^2 + v_a^2 - \omega^2) + 4v_a^2\omega^2]]} \\ D_{XXII} &= \frac{(\omega_{CXX}\omega_{CXX}u_a(\omega_{Ca}^2 + v_a^2 - 3\omega^2) - \omega_{CXX}(v_a^2 + \omega^2)(\omega_{Ca}^2 + v_a^2 - \omega^2)}{((\omega^2 + v_a^2)[((\omega_{Ca}^2 + v_a^2 - \omega^2) + 4v_a^2\omega^2]]} \\ D_{XXII} &= \frac{(\omega_{CXX}\omega_{CXX}u_a(\omega_{Ca}^2 + 3v_a^2 - 3\omega^2) - \omega_{CXX}(v_a^2 + \omega^2)(\omega_{Ca}^2 + v_a^2 - \omega^2)}{((\omega^2 + v_a^2)[((\omega_{Ca}^2 + v_a^2 - \omega^2) + 4v_a^2\omega^2]]} \\ D_{XXII} &= \frac{(\omega_{CXX}\omega_{CXX}u_a(\omega_{Ca}^2 + 3v_a^2 - 3\omega^2) + \omega_{CXX}u_a(\omega_{Ca}^2 + \omega^2) + \omega^2(\omega_{Ca}^2 + \omega^2)}{((\omega^2 + v_a^2)[((\omega_{Ca}^2 + v_a^2 - \omega^2) + 4v_a^2\omega^2]} \\ D_{XXII} &= \frac{(\omega_{CXX}\omega_{CXX}u_a(\omega_{Ca}^2 + 3\omega_{CX}^2 + 2\omega^2) + \omega_{CXX}u_a(\omega_{Ca}^2 + 2\omega^2) + \omega^2(\omega_{Ca}^2 + \omega^2)}{((\omega^2 + v_a^2)[((\omega_{Ca}^2 + v_a^2 - \omega^2) + 4v_a^2\omega^2]} \\ D_{XXII} &= \frac{(\omega_{CXX}\omega_{CXX}u_a(\omega_{Ca}^2 + v_a^2 - 3\omega^2) + \omega_{CXX}(v_a^2 + 2\omega^2)}{((\omega^2 + v_a^2)[((\omega_{Ca}^2 + v_a^2 - \omega^2) + 4v_a^2\omega^2]} \\ D_{XXII} &= \frac{(\omega_{CXX}\omega_{CXX}u_a(\omega_{Ca}^2 + v_a^2 - 3\omega^2) + \omega_{CXX}u_a(\omega_{Ca}^2 + v_a^2 - \omega^2)}{((\omega^2 + v_a^2)[((\omega_{Ca}^2 + v_a^2 - \omega^2) + 4v_a^2\omega^2]} \\ D_{XXII} &= \frac{(\omega_{CXX}\omega_{CXX}u_a(\omega_{Ca}^2 + v_a^2 - 3\omega^2) + \omega_{CXX}u_a(\omega_{Ca}^2 + v_a^2 - \omega^2)}{((\omega^2 +$$

$$\begin{split} D_{zzaR} &= \frac{(v_a^3(v_a^2 + \omega_{ca}^2 + \omega_{cza}^2 + 2\omega^2) + v_a[\omega_{cza}^2(\omega_{ca}^2 - 3\omega^2) + \omega^2(\omega_{ca}^2 + \omega^2)]}{(\omega^2 + v_a^2)[(\omega_{ca}^2 + v_a^2 - \omega^2) + 4v_a^2\omega^2]} \\ D_{zzaI} &= \left[\frac{v_a^2\omega(v_a^2 - \omega_{ca}^2 + 3\omega_{cza}^2 + 2\omega^2) + \omega(\omega_{ca}^2 - \omega^2)(\omega_{cza}^2 - \omega^2)}{(\omega^2 + v_a^2)[(\omega_{ca}^2 + v_a^2 - \omega^2) + 4v_a^2\omega^2]} \right]. \end{split}$$

b) Tensor elements of electrical conductivity

$$\sigma_{xx} = \Gamma \sigma_0 [\omega_{cy}^2 + (\nu - i\omega)^2],$$

$$\sigma_{xy} = \Gamma \sigma_0 [\omega_{cx}\omega_{cy} - \omega_{cz}(\nu - i\omega)],$$

$$\sigma_{xz} = \Gamma \sigma_0 [\omega_{cx}\omega_{cz} + \omega_{cy}(\nu - i\omega)],$$

$$\sigma_{yx} = \Gamma \sigma_0 [\omega_{cx}\omega_{cy} + \omega_{cz}(\nu - i\omega)],$$

$$\sigma_{yy} = \Gamma \sigma_0 [\omega_{cx}\omega_{cy} + (\nu - i\omega)^2],$$

$$\sigma_{yz} = \Gamma \sigma_0 [\omega_{cy}\omega_{cz} - \omega_{cx}(\nu - i\omega)],$$

$$\sigma_{zx} = \Gamma \sigma_0 [\omega_{cx}\omega_{cz} - \omega_{cy}(\nu - i\omega)],$$

$$\sigma_{zy} = \Gamma \sigma_0 [\omega_{cy}\omega_{cz} + \omega_{cx}(\nu - i\omega)],$$

$$\Gamma = [\omega_{cx}^2 + \omega_{cy}^2 + \omega_{cz}^2 + (\nu - i\omega)]^{-1}.$$